BIOCHEMISTRY
including biophysical chemistry & molecular biology

Article

pubs.acs.org/biochemistry

Kinetics of Presynaptic Filament Assembly in the Presence of Single-Stranded DNA Binding Protein and Recombination Mediator Protein

Jie Liu,[†,§] Christopher L. Berger,[‡] and Scott W. Morrical*[,†]

[†]Department of Biochemistry and [‡]Department of Molecular Physiology and Biophysics, University of Vermont College of Medicine, Burlington, Vermont 05405, United States

ABSTRACT: Enzymes of the RecA/Rad51 family catalyze DNA strand exchange reactions that are important for homologous recombination and for the accurate repair of DNA double-strand breaks. RecA/Rad51 recombinases are activated by their assembly into presynaptic filaments on single-stranded DNA (ssDNA), a process that is regulated by ssDNA binding protein (SSB) and mediator proteins. Mediator proteins stimulate strand exchange by accelerating the rate-limiting displacement of SSB from ssDNA by the incoming recombinase. The use of mediators is a highly conserved strategy in recombination, but the precise mechanism of mediator activity is unknown. In this study, the well-defined bacteriophage T4 recombination system (UvsX recombinase, Gp32 SSB, and UvsY mediator) is used to examine the kinetics of presynaptic filament assembly on native ssDNA *in vitro*. Results indicate that the ATP-dependent assembly of UvsX presynaptic filaments on Gp32-covered ssDNA is limited by a salt-sensitive nucleation step in the absence of mediator. Filament nucleation is selectively enhanced and rendered salt-resistant by mediator protein UvsY, which appears to stabilize a prenucleation complex. This mechanism potentially explains how UvsY promotes presynaptic filament assembly at physiologically relevant ionic strengths and Gp32 concentrations. Other data suggest that presynaptic filament assembly involves multiple nucleation events, resulting in many short UvsX–ssDNA filaments or clusters, which may be the relevant form for recombination *in vivo*. Together, these findings provide the first detailed kinetic model for presynaptic filament assembly involving all three major protein components (recombinase, mediator, and SSB) on native ssDNA.

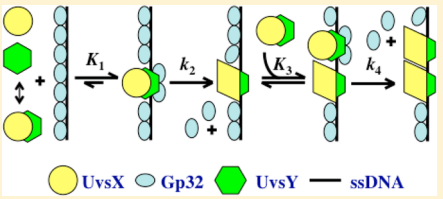

The RecA/Rad51 family of proteins is highly conserved, and its members play central roles in homologous recombination-dependent DNA repair, in support of stalled/collapsed replication forks. RecA/Rad51 enzymes catalyze DNA strand exchange, which is the pairing and physical transfer of strands between homologous DNA molecules. Strand exchange requires the formation of a presynaptic filament consisting of recombinase cooperatively bound to single-stranded DNA (ssDNA).[1] Errors in presynaptic filament assembly cause genome instability and sensitivity to DNA-damaging agents.[2] Humans with defective presynapsis are predisposed to cancer.[3]

The formation of recombinase–ssDNA filaments is regulated by other proteins, including ssDNA binding proteins (SSBs) and recombination mediator proteins (RMPs).[4] Both protein classes are highly conserved at the functional level. Biochemical studies of different recombination systems have revealed a common mechanism of presynapsis in which (1) an SSB binds to and removes secondary structure from ssDNA and (2) an RMP then mediates loading of recombinase onto the SSB–ssDNA complex with concomitant release of SSB.[4−6] The RMP stimulates DNA strand exchange by accelerating the rate-limiting displacement of SSB from ssDNA by the incoming recombinase.

Studies of the bacteriophage T4 recombination system have provided important insights into the biochemical mechanism of presynaptic filament assembly and the nature of RMP function.[4−14] UvsX protein, the RecA/Rad51 ortholog of T4 phage, exhibits both ssDNA-dependent ATPase and DNA strand exchange activities. Gp32, the phage SSB, binds tightly and cooperatively to ssDNA. UvsY, the phage RMP, stimulates UvsX activities by overcoming Gp32 inhibition and promoting its assembly onto ssDNA. Protein requirements for DNA strand exchange activity vary as a function of ionic conditions.[7,14,15] Under low-salt conditions, UvsX and Gp32 proteins are sufficient for *in vitro* strand exchange, while UvsY is dispensable. However, under high-salt conditions that approximate the *in vivo* ionic strength, UvsY is absolutely required for strand exchange along with UvsX and Gp32. *In vivo*, *uvsY* and *uvsX* mutants are equally deficient in recombination and repair functions, indicating that the mediator activity of UvsY is essential for UvsX biological function.[16,17] Previous studies revealed that UvsY successively destabilizes Gp32–ssDNA interactions and stabilizes UvsX–ssDNA interactions.[8,9] Results suggest that UvsY-induced changes in ssDNA structure play a major role in modulating the ssDNA binding activities of UvsX and Gp32.[7−9]

RMP-dependent assembly of recombinase filaments on SSB-covered ssDNA is a common feature of all recombination systems, but the mechanism by which filaments nucleate and propagate on the SSB–ssDNA complex is poorly understood. To address this problem, we developed a real-time assay for the

Received: August 5, 2013
Revised: October 8, 2013
Published: October 14, 2013

dx.doi.org/10.1021/bi401060p | *Biochemistry* 2013, 52, 7878−7889

Scheme 1. Model for Gp32F−ssDNA Association Kinetics

$$\mathrm{Gp32F} + \mathrm{ssDNA} \underset{k_{-1}}{\overset{k_1}{\rightleftharpoons}} \mathrm{Gp32F \bullet ssDNA_{isolated}} \qquad \text{Step 1: Nucleation}$$

$$\mathrm{Gp32F \bullet ssDNA_{isolated}} + \mathrm{Gp32F} \underset{k_{-2}}{\overset{k_2}{\rightleftharpoons}} \mathrm{Gp32F \bullet ssDNA_{contiguous}} \qquad \text{Step 2: Growth}$$

$$\mathrm{Gp32F \bullet ssDNA_{contiguous}} \xrightarrow{k_\tau} \mathrm{Gp32F \bullet ssDNA_{equilibrium\ cluster\ redistribution}} \qquad \text{Step 3: Isomerization}$$

Scheme 2. Nucleation−Growth Kinetic Model for UvsX Presynaptic Filament Assembly on Gp32F-Covered ssDNA

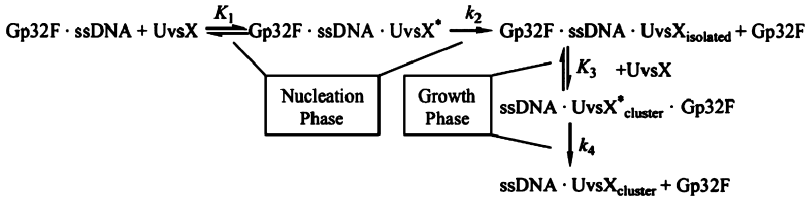

kinetics of T4 presynaptic filament assembly on Gp32-covered ssDNA, based on changes in the fluorescence of a fluorescein−Gp32 conjugate.[6] In the study presented here, we use this assay to determine kinetic parameters for the nucleation and growth of UvsX filaments on Gp32-covered ssDNA, as functions of salt, UvsY, and nucleotide ligand. The data show that UvsY selectively enhances filament nucleation by stabilizing a salt-sensitive prenucleation complex, allowing UvsX assembly and Gp32 displacement to occur at higher salt concentrations. The displacement of Gp32 from ssDNA by incoming UvsX appears to be an active process requiring the ATP-bound form of the recombinase. Other results suggest that short UvsX−ssDNA filaments resulting from multiple nucleation events are sufficient for recombination. Collectively, the data shed new light on the mechanism of presynaptic filament assembly during homologous recombination, and the critical role of recombination mediator proteins in this conserved pathway.

MATERIALS AND METHODS

Reagents. T4 proteins and M13mp18 ssDNA were prepared as described previously.[6] All ssDNA concentrations are given in nucleotide residues. 6-Iodoacetamidofluorescein-labeled Gp32 protein (Gp32F^a) was prepared as described previously.[6] Buffer A contained 20 mM Tris-HCl (pH 7.4), 3 mM $MgCl_2$, and NaCl as indicated.

Stopped-Flow Fluorescence Assays. Rapid kinetics assays were performed in a μSFM-20 stopped-flow fluorometer (BioLogic Science Instruments, Claix, France) having a dead time of 1.2 ms. This instrument was used for all measurements of Gp32F−ssDNA association kinetics and for initial studies of displacement of Gp32F from ssDNA by UvsX with or without UvsY. All protein and ssDNA concentrations reported are final concentrations after mixing. Reactions were conducted at 25 °C in buffer A with NaCl as indicated. The excitation wavelength was 460 nm with a 5 nm slit. Emission was monitored at wavelengths of >495 nm using a long-pass-cutoff filter and a 20 nm slit. Each data trace is the average of 10 independent reactions.

Gp32F−ssDNA association kinetics were modeled according to Scheme 1, which parallels the scheme derived previously for native Gp32.[18] The fluorescence traces were fit to double exponentials according to eq 1.

$$F(t) = F_\infty - A_1 \exp(-k_{obs1}t) - A_2 \exp(-k_{obs2}t) \qquad (1)$$

where $F(t)$ is the fluorescence intensity at time t, F_∞ is the fluorescence intensity at infinite time, A_1 and A_2 are the amplitudes of the first and second relaxation processes, respectively, and k_{obs1} and k_{obs2} are the observed rate constants of the first and second relaxation processes, respectively. The standard deviations of k_{obs1} and k_{obs2} reflect the associated uncertainties or fluctuations.

The observed rate constant of the first (fast) relaxation process from the double exponential (eq 1) was fit into eqs 2 and 3 to obtain the apparent forward and reverse rate constants and to calculate the equilibrium association constant for Gp32F cluster formation on the ssDNA lattice.

$$k_{obs1} = k_2(\mathrm{app})[\mathrm{ssDNA}] + k_{-2}(\mathrm{app}) \qquad (2)$$

$$K_2 = k_2(\mathrm{app})/k_{-2}(\mathrm{app}) \qquad (3)$$

Gp32F Displacement Assays for Presynaptic Filament Assembly. The kinetics of displacement of Gp32F from ssDNA by UvsX with or without UvsY were studied in a Quantamaster QM-6 steady state fluorometer (PTI). The QM-6 yielded higher sensitivity and little loss of information compared to identical experiments in a BioLogic μSFM-20 stopped-flow fluorometer, because of the slow reaction rates involved. The excitation wavelength was 460 nm with a 1 nm slit, and the emission wavelength was 519 nm with a 5 nm slit. A long-pass cutoff filter at 495 nm was used for the collection of emission data. The effects of dilution, solution change, photobleaching, inner filter, and intrinsic protein fluorescence on experimental data were evaluated as described previously[6] and were found to be negligible under the experimental conditions employed. Starting solutions containing 0.5 μM Gp32F and 3.5 μM ssDNA were preincubated at 25 °C in buffer A with NaCl and nucleotides as indicated. ATP-containing reaction mixtures also contained an ATP-regenerating system (5 mM phosphoenolpyruvate and 2.6 units/mL pyruvate kinase). UvsX and UvsY proteins were separately preincubated in the same buffer/nucleotide solution and then manually mixed into the starting solution to initiate the reaction and data collection (dead time of ≈3 s). The final concentrations of UvsX and UvsY in each experiment are indicated. Emission traces were collected at a rate of three points per second. Reported observed rate constants are averages obtained from two or three separate reactions.

Data Analysis. All fluorescence traces were fit to double exponentials using Datafit (Oakdale Engineering) according to eq 4

dx.doi.org/10.1021/bi401060p | Biochemistry 2013, 52, 7878−7889

$$F(t) = F_\infty - A_1 \exp(-k_{obs1}t) + A_2 \exp(-k_{obs2}t) \quad (4)$$

where $F(t)$ is the fluorescence intensity at time t, F_∞ is the fluorescence intensity at infinite time, A_1 and A_2 are the amplitudes of the first and second relaxation processes, respectively, and k_{obs1} and k_{obs2} are the observed rate constants of the first and second relaxation processes, respectively. The standard deviations of k_{obs1} and k_{obs2} reflect the associated uncertainties or fluctuations.

Kinetic traces of Gp32F displacement by UvsX under various conditions were fit to eq 4 to obtain observed rate constants for a fast fluorescence-increasing phase (k_{obs1}) and a slow fluorescence-decreasing phase (k_{obs2}). Both observed rate constants exhibit a hyperbolic dependence on UvsX concentration. A simplified mechanistic model for the displacement of Gp32F from ssDNA by UvsX is shown in Scheme 2, with two separated phases, filament nucleation (K_1 and k_2) and filament growth (K_3 and k_4). This simplified model is consistent with the two-step model (nucleation and growth) obtained from a recent single-molecule study of RecA filament formation on SSB-covered ssDNA.[19] This model makes the simplifying assumptions that under the experimental conditions used (1) all UvsX is saturated with ATP (or ATPγS), (2) isomerization steps k_2 and k_4 are slow and essentially irreversible, and (3) all UvsX is bound to UvsY (when present) and corresponding kinetic parameters are those of the UvsX−UvsY complex (stoichiometry undefined). Kinetic parameters in Scheme 2 were estimated by fitting k_{obs1} and k_{obs2} values obtained at different UvsX concentrations to eqs 5 and 6, respectively:

$$k_{obs1} = k_2 \frac{K_1[\text{UvsX}]}{1 + K_1[\text{UvsX}]} + k_{-2} \quad (5)$$

$$k_{obs2} = k_4 \frac{K_3[\text{UvsX}]}{1 + K_3[\text{UvsX}]} + k_{-4} \quad (6)$$

Global Fitting Method in Kinetic Data Analysis. As an independent method for estimating kinetic parameters, kinetic traces obtained at different UvsX concentrations were globally fit to differential equations derived from the model in Scheme 3, using DynaFit (BioKin Ltd.).[20] Scheme 3 is identical to Scheme 2 but contains term substitutions to facilitate mathematical modeling. The differential equations derived from Scheme 3 are

$$d[S1]/dt = -k_1[S1][S2] + k_{-1}[N1] - k_3[S1][N2] + k_{-3}[F1] \quad (7.1)$$

$$d[S2]/dt = -k_1[S1][S2] + k_{-1}[N1] \quad (7.2)$$

$$d[N1]/dt = k_1[S1][S2] - k_{-1}[N1] - k_2[N1] \quad (7.3)$$

$$d[N2]/dt = k_2[N1] - k_3[S1][N2] + k_{-3}[F1] \quad (7.4)$$

$$d[F1]/dt = k_3[S1][N2] - k_{-3}[F1] - k_4[F1] \quad (7.5)$$

$$d[F2]/dt = k_4[F1] \quad (7.6)$$

In reaction mixtures containing UvsY, all UvsX is assumed to be complexed with UvsY, because the two proteins are preincubated together and are known to interact strongly under the range of buffer conditions used in these experiments. Therefore, [S1] becomes the concentration of the free UvsX−UvsY complex, and all other UvsX-containing terms likewise include UvsY. Scheme 3 (Scheme 2) further assumes the following because of the experimental conditions. (1) UvsX is saturated with ATP (or ATPγS) because the nucleotide concentration is higher than K_m or K_d[22,23] and because experiments with ATP employ a regenerating system to maintain a high ATP/ADP ratio. (2) The level of free ssDNA in the system is negligible (all of the ssDNA is covered either with Gp32F or with UvsX and/or UvsY). This assumption is reasonable because Gp32F binds stoichiometrically to mixed sequence ssDNA under the range of buffer conditions used in these experiments,[6] and the concentration of Gp32F is saturating with respect to the total ssDNA concentration. (3) Steps k_2 and k_4 are essentially irreversible ($k_{-2} = k_{-4} = 0$), so that once Gp32F is displaced from ssDNA, it does not compete with UvsX for ssDNA binding sites. This assumption derives from the pre-steady state conditions, including the fact that UvsX with or without UvsY is added to a preassembled Gp32F−ssDNA complex, such that the concentration of free Gp32F is essentially zero at early stages of each reaction and therefore cannot compete. Also, it was observed empirically that the reoccupation of ssDNA by Gp32F requires the hydrolytic depletion of ATP by UvsX, which is prevented in these reactions either by using a regenerating system or by using ATPγS.

During global fitting using DynaFit, iterative runs for individual isotherms were taken to determine the values and standard errors of rate constants k_2, k_4, k_1, and k_3 sequentially, according to eq 7. To facilitate convergence, rate constants k_{-1} and k_{-3} were each assigned a value of 1 s^{-1} and were held constant in all iterations; therefore, only the association constants for the equilibrium steps, K_1 ($=k_1/k_{-1}$) and K_3 ($=k_3/k_{-3}$), are reported in Table 3. K_1 and K_3 values determined at 50 mM NaCl are similar in magnitude to estimates of UvsX−ssDNA binding affinity under equilibrium binding conditions (ref 4 and unpublished results of H. Xu and S. Morrical). The fitting quality can be judged by Figure 4 and by the standard errors of the kinetic constants in Table 3. In

Scheme 3. Symbolic Representation of Scheme 2, Used for Global Fitting of Model-Derived Differential Equations[a]

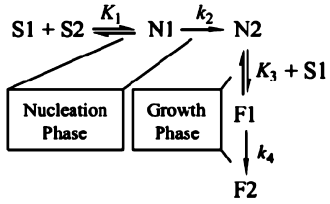

[a]This is identical to Scheme 2 but contains the following term substitutions to facilitate mathematical modeling. [S1] represents the concentration of free UvsX protein. [S2] represents the concentration of Gp32F-covered ssDNA that is converted to all available binding sites for UvsX, according to a binding site size (n) of four nucleotide residues.[21] [N1] represents the concentration of an initial Gp32F−ssDNA−UvsX* prenucleation complex in which UvsX binds Gp32F-covered ssDNA to form isolated sites. [N2] represents the concentration of the Gp32F−ssDNA−$\text{UvsX}_{\text{isolated}}$ complex, an isomerized productive form of nucleation complex in which UvsX forms isolated stable sites on Gp32F-covered ssDNA. [F1] represents the concentration of a ssDNA−$\text{UvsX*}_{\text{Cluster}}$−Gp32F filament intermediate in which UvsX forms initial clusters on Gp32F-covered ssDNA. [F2] represents the concentration of the ssDNA−$\text{UvsX}_{\text{Cluster}}$ isomerized productive cluster in which UvsX forms a productive presynaptic filament on ssDNA.

dx.doi.org/10.1021/bi401060p | Biochemistry 2013, 52, 7878−7889

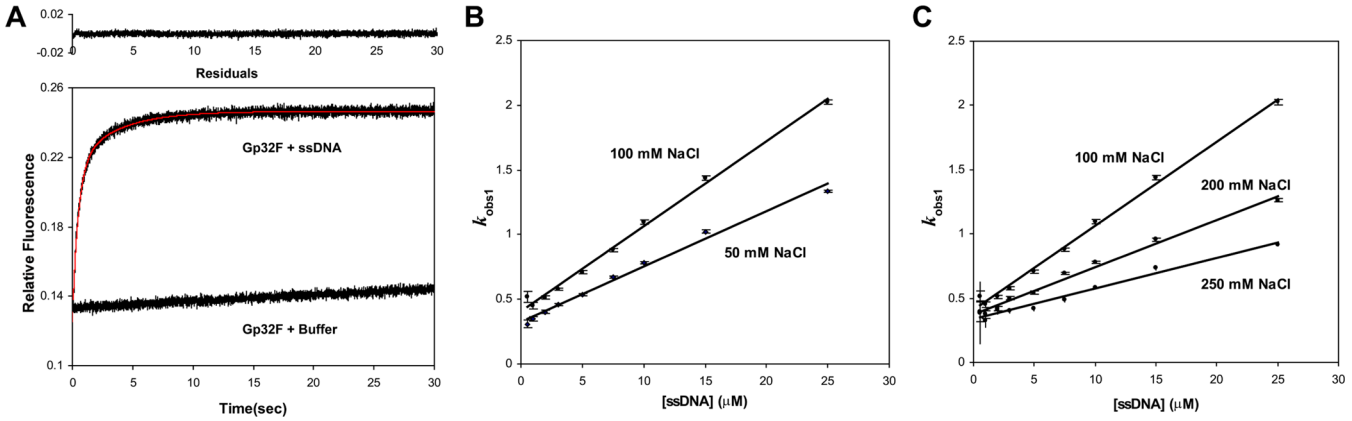

Figure 1. (A) Time course of rapid association between 25 μM M13mp18 ssDNA and 0.5 μM Gp32F, shown in black. The red curve represents the double-exponential fit of the data according to eq 1 (k_{obs1} = 2.02 ± 0.02 s^{-1}, and k_{obs2} = 0.292 ± 0.003 s^{-1}), and the residuals are colored black at the top. The buffer control with only 0.5 μM Gp32F is shown as the black trace at the bottom, containing buffer A with 100 mM NaCl, at 25 °C. (B and C) Gp32F−M13mp18 ssDNA association as a function of NaCl concentration under both strong (B) and weak (C) binding conditions. All the reaction mixtures used to produce the data depicted in panels B and C contained 0.5 μM Gp32F and various amounts of M13mp18 ssDNA in buffer A with the indicated NaCl concentration. The kinetic parameters from fitting (see the text) are summarized in Table 1, which reflect the apparent on and off rates in the second step in the Lohman model, as shown in Scheme 1.[18]

nearly all cases, the hyperbolic and global fitting methods yielded similar estimates of kinetic parameters K_1, k_2, K_3, and k_4.

RESULTS

Kinetic Properties of Gp32F−ssDNA Interactions. Fluorescein-conjugated Gp32 (Gp32F) exhibits a fluorescence increase upon binding to ssDNA, and its equilibrium ssDNA binding properties are a reasonable approximation of unlabeled Gp32.[6] These properties make Gp32F a useful real-time probe for T4 presynaptic filament assembly. To establish the kinetic studies of assembly of the UvsX−ssDNA complex on Gp32-covered ssDNA, we first investigated the basic kinetic properties of Gp32F−ssDNA binding using stopped-flow fluorescence. Gp32F−ssDNA binding follows the same three-step mechanism previously derived for unlabeled Gp32 (Scheme 1 and Figure 1A):[18] (1) a very fast nucleation step (too fast to detect) with a small amplitude during which Gp32F nucleates onto the lattice and forms isolated binding sites, (2) a fast growth step with a large amplitude during which Gp32F propagates onto the lattice and forms contiguous clusters, and (3) a slow isomerization step with a small amplitude during which the contiguous Gp32F protomers are redistributed by facilitated diffusion to form stable clusters on the lattice.

Figure 1A shows a typical kinetic trace for the case in which Gp32F is rapidly mixed with excess ssDNA. The time-dependent fluorescence change of Gp32F fits a double-exponential function (eq 1) similar to that of wild-type Gp32.[18] The rate constant of the fast phase, k_{obs1}, was assigned to the growth step (step 2 in Scheme 1) on the basis of its large amplitude. To obtain rate constants, we performed a series of rapid binding experiments under different salt conditions, with constant Gp32F and variable ssDNA concentrations. At low salt concentrations, strong binding conditions (50−100 mM NaCl), the observed growth rate constant, k_{obs1} (step 2 in Scheme 1), increases with increasing salt concentration (Figure 1B). At high salt concentrations, weak binding conditions (100−250 mM NaCl), k_{obs1} decreases with an increasing salt concentration (Figure 1C). The effects of salt on Gp32F−ssDNA binding kinetics parallel those of unlabeled Gp32.[18] Under low-salt conditions, k_{obs1} increases with an increasing salt concentration because Na^+ disrupts electrostatic interactions between the C-terminal and core domains of Gp32 that inhibit DNA binding.[27] Under high-salt conditions, k_{obs1} decreases with an increasing salt concentration because a higher salt concentration interrupts protein−DNA electrostatic interactions.

As shown in panels B and C of Figure 1, k_{obs1} exhibits a linear dependence on ssDNA concentrations under all salt conditions. Apparent on and off rate constants for the growth step, k_2(app) and k_{-2}(app), respectively, were obtained from linear fits of these data to eq 2. The apparent association rate has a much stronger dependence on NaCl concentration [d log k_2(app)/d log[NaCl] = −0.75 ± 0.01] than the apparent dissociation rate [d log k_{-2}(app)/d log[NaCl] = −0.19 ± 0.01], when the NaCl concentration is increased from 100 to 250 mM. In the same salt interval, the equilibrium affinity of Gp32F, K_{ss}, decreased from 1.6×10^5 to 7.1×10^4 M^{-1}, and the d log K_{ss}/d log[NaCl] value is equal to −0.83 ± 0.03. The substrate for Gp32F filament assembly is natural phage ssDNA under no tension, and our results indicate the impact of salt on the electrostatic interactions between Gp32 and ssDNA can be attributed to a decrease in the association rate, not an increase in the dissociation rate.

The rate constants and calculated association constants (eq 3) are summarized in Table 1 for comparison with those of unlabeled Gp32. Gp32F displays a 50-fold decrease in k_2(app) for binding M13mp18 ssDNA, compared to that of unlabeled Gp32 binding poly(rεA).[18] We previously reported that Gp32F shows a 12-fold decrease in its intrinsic binding affinity for M13mp18 ssDNA compared to that of unlabeled Gp32.[6] Additionally, Gp32 displays a lattice bias favoring homopolymers and etheno-modified bases (J. Liu and S. W. Morrical, unpublished results). Overall, the data indicate that Gp32F−ssDNA binding follows the same kinetic mechanism (Scheme 1) as unlabeled Gp32, and that the lower affinity of Gp32F for ssDNA versus that of Gp32 is largely due to its slower growth on rate. For these reasons, following the UvsX-dependent displacement of Gp32F from preassembled Gp32F−ssDNA complexes provides relevant information about the kinetics of

dx.doi.org/10.1021/bi401060p | Biochemistry 2013, 52, 7878−7889

Table 1. Effects of NaCl Concentration on the Kinetic Parameters of Binding of Gp32F to ssDNA[a]

[NaCl] (mM)	Gp32F		Gp32 (from ref 18)	
	k_2(app) (M^{-1} s^{-1})	k_{-2}(app) (s^{-1})	K_2 (M^{-1})	k_2 (M^{-1} s^{-1})
50	$(4.3 \pm 0.2) \times 10^4$	0.33 ± 0.02	1.3×10^5	1.3×10^6
100	$(6.6 \pm 0.2) \times 10^4$	0.41 ± 0.02	1.6×10^5	2.8×10^6
200	$(3.7 \pm 0.1) \times 10^4$	0.37 ± 0.02	1.0×10^5	–
250	$(2.4 \pm 0.1) \times 10^4$	0.34 ± 0.02	7.1×10^4	–

[a]The apparent rate constants k_2 and k_{-2} and the calculated equilibrium constant K_2 for Gp32F–ssDNA interactions were derived from linear fits of the data in panels B and C of Figure 1 as described in Materials and Methods. Previously published values of k_2 for interactions of unmodified Gp32 with a poly(rεA) lattice are shown for comparison.

presynaptic filament assembly on the native Gp32–ssDNA complex.

Presynaptic Filament Assembly as a Function of Salt, Nucleotide, and UvsY. UvsX–ssDNA filament assembly was monitored by the displacement of Gp32F from ssDNA with a concomitant fluorescence decrease.[6] Preassembled Gp32F–ssDNA complexes were rapidly mixed with a stoichiometric amount of UvsX in buffer A with 50 mM NaCl and various nucleotides (Figure 2A). Under these conditions, filament assembly is UvsY-independent, because of the differential salt effects on Gp32–ssDNA versus UvsX–ssDNA interactions (see Discussion). This property is shown clearly by the data in Figure 2A, wherein the addition of UvsX to a preformed Gp32F–ssDNA complex in the absence of UvsY leads to a time-dependent decrease in Gp32F fluorescence. The displacement of Gp32F requires ATP binding but not ATP hydrolysis by UvsX, because the change in signal occurs in the presence of either ATP or ATPγS, but not in the presence of ADP, AMP, or no nucleotide (Figure 2A). The substrate analogue ATPγS is very slowly hydrolyzed by UvsX and stabilizes UvsX–ssDNA interactions.[21,22] Note that ATP and ATPγS, when present, were at saturating concentrations,[22,23] and that an ATP regenerating system was included to maintain a high ATP/product ratio throughout the time course. The latter measure was necessary to prevent the dissociation of UvsX from ssDNA caused by the buildup of ATP hydrolytic products, which eventually leads to the reoccupation of ssDNA by Gp32F.[6]

An increasing salt concentration inhibits presynaptic filament assembly in the absence of UvsY (Figure 2B). All of the reactions in Figure 2B were performed in the presence of a saturating level of ATP and an ATP regenerating system. Increasing the NaCl concentration from 50 to 100 mM causes a sharp decrease in the rate of Gp32F displacement, while 200 mM NaCl blocks the reaction entirely. The addition of UvsY protein restores filament assembly at 200 mM NaCl, however (Figure 2B). These observations are consistent with the effects of salt and UvsY on the *in vitro* DNA strand exchange activity of UvsX.[7,14] The data may also explain why T4 recombination transactions are codependent on UvsX and UvsY *in vivo*,[17] where the ionic strength is relatively high.

Filament Nucleation Is Rapid but Salt-Sensitive. Kinetic traces in the presence of nucleoside triphosphate and at low salt concentrations (Figure 2) were fit accurately by a double-exponential function with increasing and decreasing phases (eq 4) to obtain the observed rate constants for the fast reaction with a small positive amplitude (designated as UvsX nucleation, k_{obs1}) and for the slow reaction with a large negative amplitude (designated as UvsX growth, k_{obs2}), as listed in Table 2. In 50 mM NaCl, ATPγS enhances UvsX's observed nucleation rate ~11-fold and the observed growth rate ~4-fold, compared to the rate with natural substrate ATP (Figure 2A and Table 2). This is consistent with the notion that ATPγS stabilizes the high-affinity ssDNA-binding conformation associated with the ATP-bound form of UvsX.[21,22] The data indicate that this form of UvsX is necessary for Gp32 displacement during both nucleation and growth phases of filament assembly. Note that observed nucleation rates are fast compared to growth rates (Table 2), suggesting that presynaptic filaments assemble from many nucleation centers on the Gp32–ssDNA complex (see Discussion).

In the presence of ATP, doubling the NaCl concentration from 50 to 100 mM causes a 2.3-fold decrease in the observed nucleation rate (k_{obs1}) but has little effect (~1.1-fold decrease) on the observed growth rate (Table 2). Therefore, salt has a

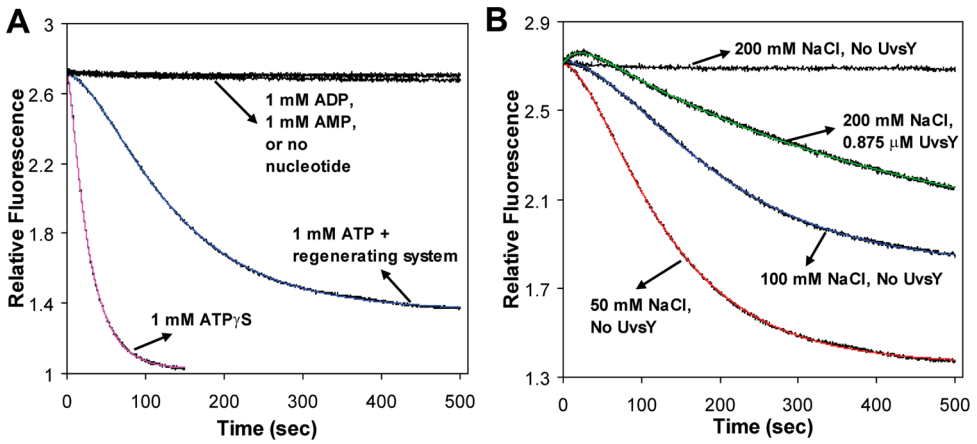

Figure 2. Displacement of Gp32F from ssDNA by UvsX is affected by nucleotides, salt, and UvsY. (A) The 0.5 μM Gp32F–3.5 μM M13mp18 ssDNA complex was rapidly mixed with 0.875 μM UvsX in buffer A with 50 mM NaCl and either no nucleotide, 1 mM AMP, 1 mM ADP, 1 mM ATP with a regenerating system (R.S.), or 1 mM ATPγS, at 25 °C. Red and blue curves represent the best fits of eq 4 to reactions with 1 mM ATP plus R.S. and 1 mM ATPγS, respectively. (B) The 0.5 μM Gp32F 3.5 μM M13mp18 ssDNA complex was rapidly mixed with 0.875 μM UvsX with or without 0.875 μM UvsY in buffer A, 1 mM ATP, R.S., and either 50, 100, or 200 mM NaCl, at 25 °C. Red, blue, and green curves represent the best fits of eq 4 to reactions with 50 mM NaCl, 100 mM NaCl, and 200 mM NaCl with UvsY, respectively. Fitting parameters are listed in Table 2.

dx.doi.org/10.1021/bi401060p | *Biochemistry* 2013, 52, 7878–7889

Table 2. Effects of Nucleotides, Salt, and UvsY Protein on the Observed Rates and Amplitudes for the Displacement of Gp32F from ssDNA by UvsX Recombinase[a]

nucleotide	[NaCl]	k_{obs1} ($\times 10^{-3}$ s^{-1})	A_1 ($\times 10^5$)	k_{obs2} ($\times 10^{-3}$ s^{-1})	A_2 ($\times 10^5$)
ATPγS	50	274 ± 11	2.5 ± 0.1	37.8 ± 0.1	19.4 ± 0.0
ATP with R.S.	50	24.4 ± 0.4	8.3 ± 0.2	9.5 ± 0.0	21.8 ± 0.2
	100	10.6 ± 0.8	5.0 ± 0.1	8.3 ± 0.5	14.5 ± 0.1
	200	<0.125	–	<0.125	–
ATP with R.S. and UvsY	200	59.1 ± 1.5	1.4 ± 0.0	2.4 ± 0.0	10.0 ± 0.0
ADP	50	<0.125	–	<0.125	–
AMP	50	<0.125	–	<0.125	–
none	50	<0.125	–	<0.125	–

[a]Observed rate constants (k) and amplitudes (A) were derived from double-exponential fits of the fluorescence traces in Figure 2 as described in the text. Reactions were conducted in buffer A containing NaCl concentrations as indicated. Nucleotides, when present, were at a concentration of 1 mM. R.S. denotes the presence of an ATP regenerating system. Concentrations of M13mp18 ssDNA, Gp32F, and UvsX were 3.5, 0.5, and 0.875 μM, respectively. UvsY, when present, was at a concentration of 0.875 μM.

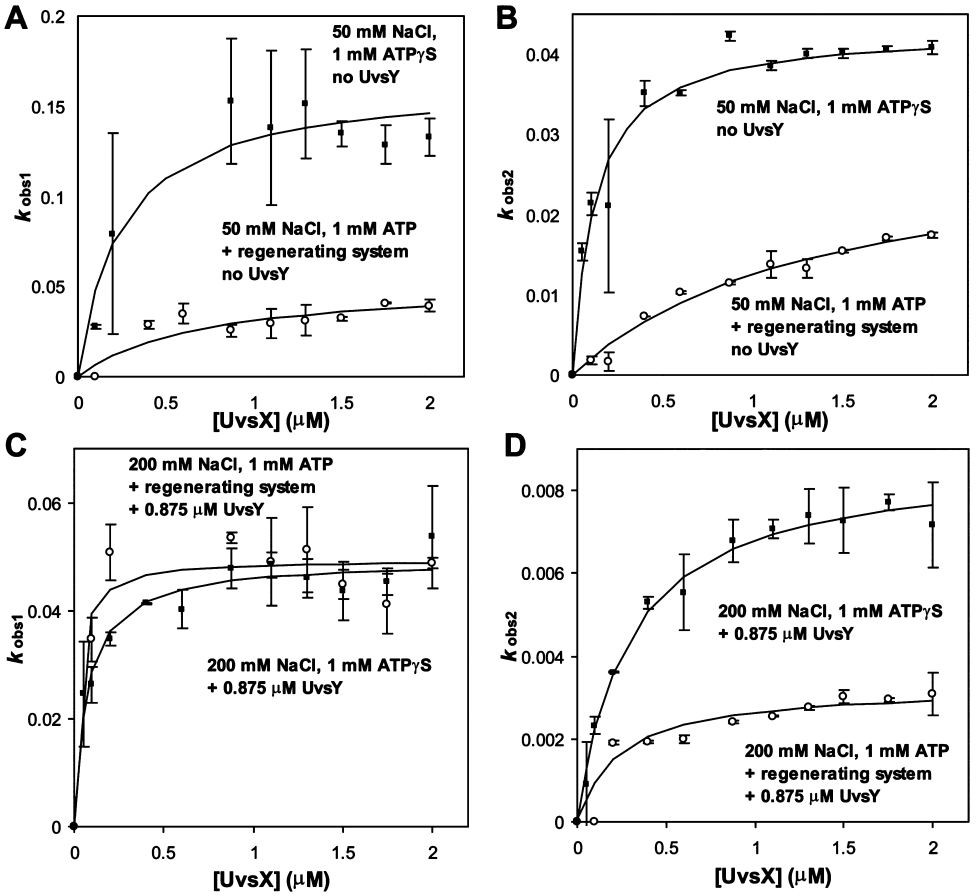

Figure 3. Pre-steady state studies of UvsX–ssDNA binding via Gp32F displacement. (A and B) Observed rate constants of (A) UvsX nucleation (k_{obs1}) and (B) UvsX growth (k_{obs2}) on the Gp32F–ssDNA complex as functions of UvsX concentration in buffer A, 50 mM NaCl, and either 1 mM ATP with R.S. or 1 mM ATPγS as indicated. For all reactions used to produce the data depicted in panels A and B, the 0.5 μM Gp32F–3.5 μM M13mp18 ssDNA complex was rapidly mixed with the indicated amount of UvsX at 25 °C. (C and D) Observed rate constants of (C) UvsX nucleation (k_{obs1}) and (D) UvsX propogation (k_{obs2}) on the Gp32F–ssDNA complex in the presence of UvsY, as a function of UvsX concentration in buffer A, 200 mM NaCl, and either 1 mM ATP with R.S. or 1 mM ATPγS as indicated. For all reactions used to produce the data depicted in panels C and D, the 0.5 μM Gp32F–3.5 μM M13mp18 ssDNA complex was rapidly mixed with the indicated amount of UvsX with 0.875 μM UvsY at 25 °C. Curves in panels A–D represent fits of the data to eqs 2 and 3. Fitting parameters are listed in Table 3.

strong effect on nucleation and a weak effect on growth. Thus, the inability of UvsX (with ATP) to displace Gp32F from ssDNA in 200 mM NaCl (Figure 2B) likely reflects a failure of UvsX to nucleate onto the Gp32F–ssDNA complex. The addition of UvsY is required for Gp32F displacement under these conditions (Figure 2B). The UvsY-dependent trace is also fit accurately by a double exponential with increasing and decreasing phases (eq 4). The observed nucleation rate, k_{obs1}, of the UvsY-dependent reaction in 200 mM NaCl is 2.4- and 5.6-fold higher than those of the UvsY-independent reactions in 50 and 100 mM NaCl, respectively (Table 2). ATP binding by UvsX is still required for the UvsY-dependent reaction, however, because no reaction is observed with ADP, AMP, or

dx.doi.org/10.1021/bi401060p | Biochemistry 2013, 52, 7878–7889

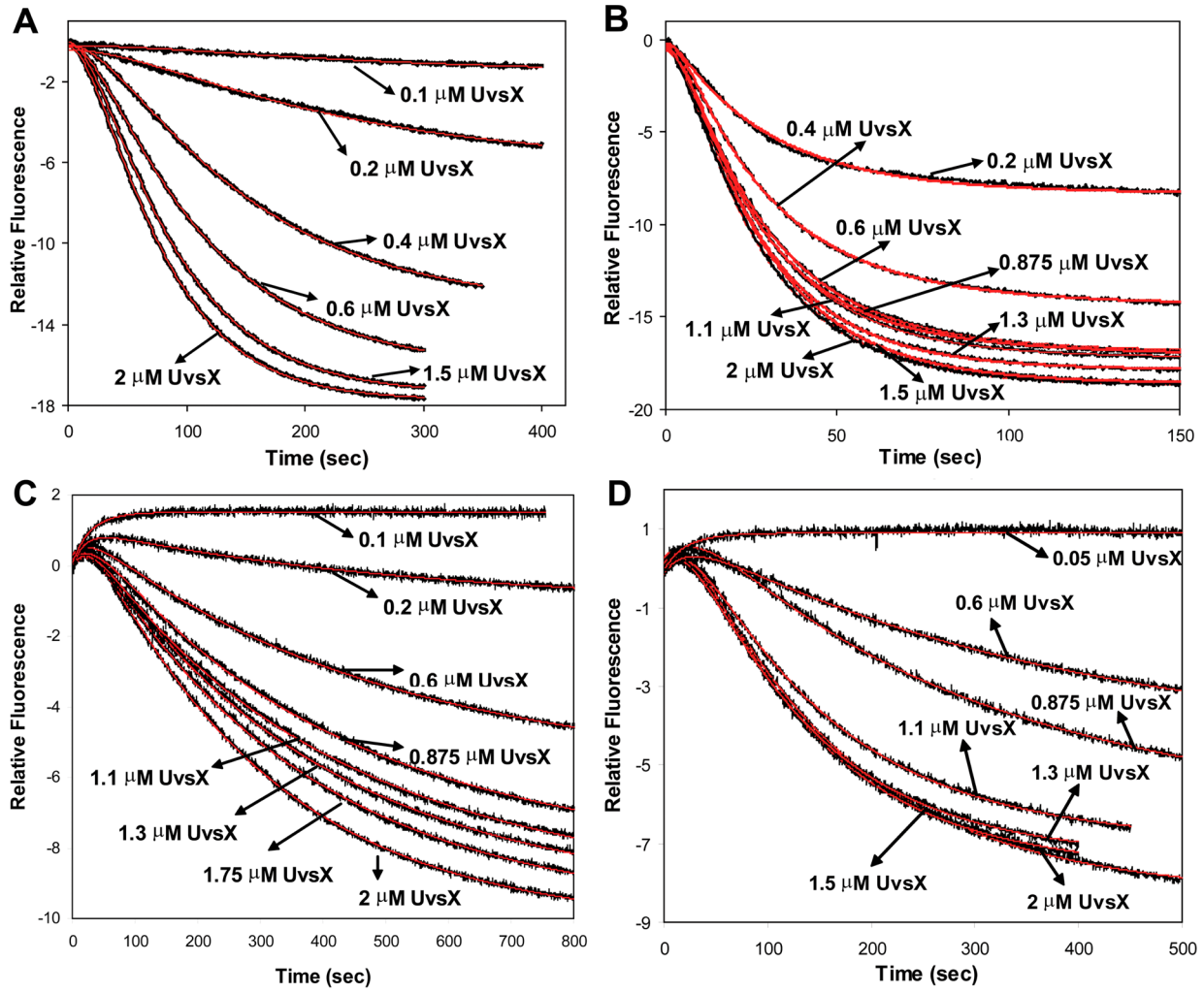

Figure 4. Time courses of Gp32F displacement by different concentrations of UvsX. Red curves represent the best stepwise global fit models (eq 7). Fitting parameters are listed in Table 3. (A and B) Reactions in buffer A, 50 mM NaCl, and either (A) 1 mM ATP with R.S. or (B) 1 mM ATPγS. For all reactions used to produce the data depicted in panels A and B, the 0.5 μM Gp32F−3.5 μM M13mp18 ssDNA complex was rapidly mixed with the indicated amount of UvsX at 25 °C. (C and D) Reactions in buffer A, 200 mM NaCl, 0.875 μM UvsY, and either (C) 1 mM ATP with R.S. or (D) 1 mM ATPγS. For all reactions used to produce the data depicted in panels C and D, the 0.5 μM Gp32F−3.5 μM M13mp18 ssDNA complex was rapidly mixed with the indicated amount of UvsX with 0.875 μM UvsY at 25 °C. During curve fitting, iterative runs for individual isotherms were taken to determine values and standard errors of kinetic constants.

no nucleotide under these conditions (ref 6 and data not shown).

Unique Fluorescence Signature of Filament Nucleation. As shown in Figure 2B, the kinetic trace of the reaction mixture containing UvsY shows a significant initial fluorescence increase, which could be fit accurately to eq 4. We attribute the initial fluorescence increase to the formation of a prenucleation complex with enhanced Gp32F fluorescence (see Discussion). This prenucleation complex is formed in the absence of UvsY, as well, because these reactions are also fit accurately by eq 4 (Figure 2A,B). In buffer containing 200 mM NaCl, where UvsX alone fails to displace Gp32F from ssDNA, the presence of UvsY increases the observed nucleation rate (k_{obs1}) by at least 470-fold over the background rate (Table 2). The observed growth rate (k_{obs2}) is 40 times slower than the observed nucleation rate (Table 2), suggesting that UvsY functions primarily to enhance nucleation rather than growth of UvsX filaments on Gp32-covered ssDNA.

Kinetic Model for Presynaptic Filament Assembly. A series of Gp32F displacement assays were conducted at different UvsX concentrations under high-salt (200 mM NaCl) or low-salt (50 mM NaCl) conditions, and in the presence of either ATPγS or ATP. In 200 mM NaCl, a constant amount of UvsY (stoichiometric with respect to ssDNA assuming a binding site size of four nucleotide residues per monomer)[24] was preincubated with variable amounts of UvsX. Under all conditions, the observed rate constants of both nucleation and growth steps appear to increase with an increasing UvsX concentration in a saturable manner (Figure 3). The data can be approximated using a relatively simple four-step model (Scheme 2): (1) a rapid binding step (K_1) during which UvsX binds the Gp32F−ssDNA complex and forms a transient prenucleation complex (Gp32F retained), (2) a slow and essentially irreversible isomerization step (k_2) during which UvsX changes conformation to form a stable nucleation site (Gp32F displaced), (3) another rapid binding step (K_3) during which UvsX forms unstable contiguous clusters (Gp32F retained), and (4) another slow and essentially irreversible isomerization step (k_4) during which UvsX clusters are redistributed into stable filaments on the lattice (Gp32F

dx.doi.org/10.1021/bi401060p | Biochemistry 2013, 52, 7878−7889

Table 3. Fitted Kinetic Parameters for the Displacement of Gp32F from ssDNA during UvsX−ssDNA Filament Assembly under Low-Salt (UvsY-independent) and High-Salt (UvsY-dependent) Conditions[a]

			nucleation		growth	
conditions		fitting method[b]	K_1 ($\times 10^6$ M^{-1})	k_2 ($\times 10^{-3}$ s^{-1})	K_3 ($\times 10^6$ M^{-1})	k_4 ($\times 10^{-3}$ s^{-1})
50 mM NaCl without UvsY	ATP and R.S.	hyperbolic	1.4 ± 0.9	53 ± 16	0.7 ± 0.2	30 ± 4
		global	2.6 ± 1.5	35 ± 4	1.5 ± 0.3	35 ± 4
	ATPγS	hyperbolic	4.1 ± 1.6	163 ± 13	8.2 ± 1.3	43 ± 1
		global	3.1 ± 1.2	337 ± 89	4.1 ± 2.7	42 ± 4
200 mM NaCl with UvsY	ATP and R.S.	hyperbolic	39 ± 26	50 ± 2	4.0 ± 1.5	3.2 ± 0.3
		global	68 ± 44	47 ± 11	3.0 ± 1.2	4.6 ± 0.6
	ATPγS	hyperbolic	14 ± 3	49 ± 2	3.5 ± 0.4	8.8 ± 0.2
		global	64 ± 32	50 ± 7	3.0 ± 1.4	11 ± 2

[a]Reactions were conducted in buffer A containing 50 mM NaCl (low-salt, UvsY-independent conditions) or containing 200 mM NaCl (high-salt, UvsY-dependent conditions). The nucleotide concentration was 1 mM in all reactions. R.S. denotes the presence of an ATP regenerating system. Concentrations of M13mp18 ssDNA and Gp32F were 3.5 and 0.5 μM, respectively. UvsY, when present, was at a concentration of 0.875 μM. Under each condition, fluorescence traces were obtained at multiple UvsX concentrations (Figure 4A−D). [b]Kinetics were modeled according to Scheme 2 using two independent data-fitting procedures (see Materials and Methods). With the hyperbolic fitting method, kinetic parameters were determined by fitting hyperbolic functions (eqs 2 and 3) to plots of k_{obs1} and k_{obs2}, respectively, vs UvsX concentration as shown in Figure 3A−D. With the global fitting method, direct global fits of fluorescence traces to model-derived differential equations (eqs 7.1−7.6) were performed using DynaFit to obtain kinetic parameters for filament nucleation and growth phases. Scheme 3, a symbolic version of Scheme 2, was used for mathematical modeling. Fitted curves are shown in Figure 4A−D.

displaced). Steps 1 and 2 comprise the nucleation phase defined by k_{obs1} and eq 5, whereas steps 3 and 4 comprise the growth phase defined by k_{obs2} and eq 6. The assumptions underlying this model are stated in Materials and Methods. Our kinetic model through ensemble studies also agrees well with previous nucleation−growth models from single-molecule studies of RecA filament formation on double-stranded DNA (dsDNA) or SSB-covered ssDNA.[19,25]

Estimates of K_1, k_2, K_3, and k_4 were obtained by fitting hyperbolic eqs 2 and 3 to plots of k_{obs1} or k_{obs2} versus UvsX concentration (Figure 3). The kinetic mechanism in Scheme 2 was tested independently via global fits of model-derived differential equations (eq 7) to raw fluorescence trace data (Figure 4). Kinetic parameters determined from both hyperbolic and global fitting methods are listed in Table 3. In nearly all cases, the two fitting methods gave very similar results [≤~2-fold difference in parameter values (Table 3)], indicating that Scheme 2 is a reasonable model for this system. The only exception was a 4.6-fold difference in K_1 obtained from global versus hyperbolic fitting methods for reactions in 200 mM NaCl with UvsY and ATPγS (Table 3). Under these conditions, the global fitting method failed to converge at intermediate UvsX concentrations (0.1−0.5 μM), indicating additional complexity in the kinetic mechanism (see Discussion).

Three major findings emerge from the data in Table 3. First, in reactions at 200 mM NaCl, the presence of UvsY strongly and specifically increases the K_1 of the nucleation phase compared to that of UvsY-independent reactions at 50 mM NaCl. The average increase is 27-fold with ATP and 11-fold with ATPγS as a cofactor. Therefore, UvsY appears to promote presynaptic filament assembly primarily by stabilizing a salt-sensitive prenucleation complex. Second, the k_4 of the growth phase appears to be rate-limiting for UvsY-dependent filament assembly at high salt concentrations (average k_4/k_2 values of 0.08 and 0.2 with ATP and ATPγS as a cofactor, respectively). The same is true for UvsY-independent reactions at low salt concentrations with ATPγS as a cofactor (average k_4/k_2 of 0.2). Third, in UvsY-independent reactions at low salt concentrations, ATPγS enhances both the k_2 of the nucleation phase and the K_3 of the growth phase by ~6-fold compared to those of reactions with ATP as a cofactor. The implications of these findings are discussed below.

DISCUSSION

Data from our ensemble measurements of T4 presynaptic filament assembly are described well by a relatively simple, nucleation−growth kinetic model (Figure 5). The model is similar to nucleation−growth models for RecA filament formation on dsDNA or the SSB−ssDNA complex that were derived from single-molecule measurements.[19,25] The utility of the model is established by the fact that hyperbolic plots of observed rate constants versus UvsX concentration (Figure 3) and global fitting of model-derived differential equations to raw fluorescence traces (Figure 4) both return similar values for kinetic parameters under almost all conditions (Table 3). Under one narrow set of conditions (intermediate UvsX concentrations in 200 mM NaCl with UvsY and ATPγS), the global fitting algorithm failed to converge, suggesting additional complexity. One possible reason for the lack of convergence is competition between the nucleation and growth phases for UvsX under these conditions. UvsY and ATPγS have been shown to stabilize UvsX−ssDNA interactions synergistically at high salt concentrations.[8] It is conceivable that this leads to a burst of nucleation events that, at relatively low UvsX concentrations, depletes it from the growth phase. This would be consistent with the idea that UvsY promotes multiple nucleation events leading to many short filaments (see below).

Mediator Protein UvsY Stabilizes a Salt-Sensitive Prenucleation Complex. As illustrated in the model (Figure 5), the critical first step (K_1) of this mechanism is the ATP-dependent formation of a prenucleation complex containing UvsX recombinase co-occupying the ssDNA along with the SSB component, Gp32. The prenucleation complex is distinguished from subsequent intermediates by its relative salt sensitivity and by fluorescence enhancement effects on a Gp32F probe. It is worth noting that the T4 helicase loading protein, Gp59, enhances the fluorescence of Gp32F within a tripartite Gp59−Gp32F−ssDNA complex.[26] The formation of this complex precedes loading of the replicative helicase, Gp41, which is accompanied by Gp32F displacement. The parallel

dx.doi.org/10.1021/bi401060p | Biochemistry 2013, 52, 7878−7889

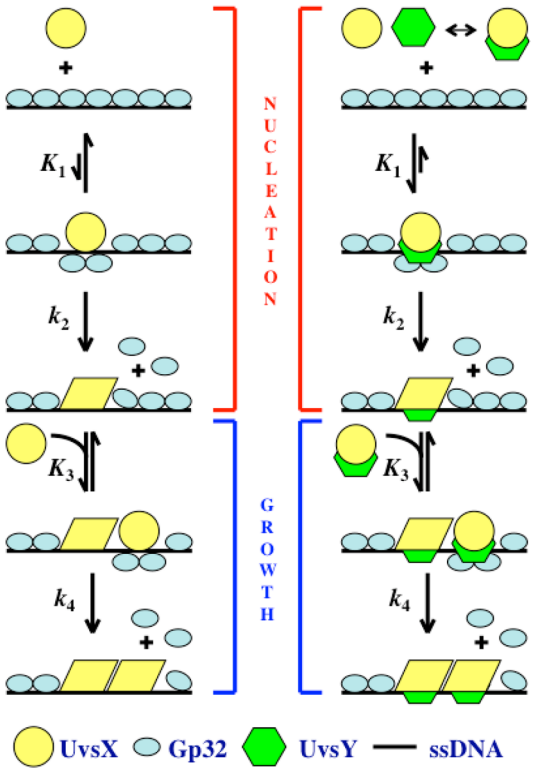

Figure 5. Model for UvsX presynaptic filament assembly on Gp32-covered ssDNA. In the left panel, under low-salt conditions in the absence of mediator protein UvsY, ATP-bound UvsX, a high-affinity form, binds the Gp32–ssDNA complex rapidly to form an unstable nucleation site or "prenucleation complex" (association constant K_1). A slow but almost irreversible conformational change (forward rate constant k_2) is required by UvsX to displace Gp32 and to secure this isolated nucleation site on the lattice. With successful nucleation, more ATP-bound UvsX is recruited to form an unstable cluster (association constant K_3). This rapidly formed UvsX cluster undergoes another slow but almost irreversible conformational change to displace Gp32 and to redistribute it into a stable and productive presynaptic filament (forward rate constant k_4). In the right panel, under high-salt conditions, the mediator protein, UvsY, facilitates filament nucleation by stabilizing the salt-sensitive prenucleation complex (enhanced K_1), by forming a special quaternary complex with UvsX, Gp32, and ssDNA. Filament growth (particularly k_4) is rate-limiting under both UvsY-dependent and -independent conditions. Therefore, filament assembly necessary for DNA strand exchange and recombination functions of UvsX likely involves frequent nucleation events leading to many short filaments. See the text for details.

fluorescence effects on Gp32F seen during UvsX loading and helicase loading suggest that transient intermediates in both processes may involve similar changes in the Gp32–ssDNA structure or environment.

The data indicate that UvsY specifically stabilizes the prenucleation complex at high salt concentrations (Table 3 and Figure 5). By overcoming the salt sensitivity of presynaptic filament nucleation, UvsY activates UvsX to perform its recombination functions under physiological conditions. The observed salt sensitivity of filament nucleation is consistent with the observation that the intrinsic affinity parameter of UvsX for ssDNA, K_{ss}, is salt-sensitive.[21] The isolated binding of UvsX to ssDNA during filament nucleation presumably depends on K_{ss} alone, while contiguous binding of UvsX to ssDNA during filament growth also depends on ω, the salt-insensitive cooperativity parameter. The salt dependence of UvsX–Gp32 exchange also reflects differential salt effects on the ssDNA binding activities of Gp32 and UvsX. Over the salt interval covered in this study (50–250 mM NaCl), the Gp32–ssDNA binding affinity is only weakly dependent on salt concentration; in fact, the affinity decreases slightly at 50 mM NaCl (Table 1).[18,27] This can be attributed to a masking effect caused by the acidic C-terminal domain of Gp32, which has been well-documented elsewhere.[27] In contrast, the ssDNA binding affinity of UvsX increases markedly with a decreasing salt concentration over the same interval, and UvsX–ssDNA interactions are further stabilized by ATP binding.[8,28] Therefore, at 50 mM NaCl, the UvsX–ATP complex possesses sufficient ssDNA binding affinity to compete with Gp32 for binding sites on ssDNA, while at 200 mM NaCl, it does not and, therefore, requires the mediator activity of UvsY.

The observed salt sensitivity of UvsX–ssDNA filament nucleation is consistent with results of single-molecule studies of *Escherichia coli* RecA–dsDNA filaments. The latter revealed a strong impact of ionic strength on nucleation cluster frequency, while the impact is much milder on the average cluster growth rate.[25] Somewhat different results were obtained in single-molecule studies of RecA filament assembly on SSB–ssDNA complexes, which found relatively modest effects of salt on filament nucleation and growth rates from 50 to 200 mM NaCl.[19] This difference could be due to the use of ATPγS in the latter study, because ATPγS greatly stabilizes RecA–ssDNA filaments at salt concentrations as high as 600 mM NaCl,[29] which likely precludes the need for a mediator protein. In contrast, UvsX–ssDNA filaments in the presence of ATP (this study) are significantly more salt-sensitive, and therefore, nucleation becomes mediator-dependent with an increasing salt concentration.

Growth Is Rate-Limiting in Presynaptic Filament Assembly. UvsX filament assembly on the Gp32–ssDNA complex is characterized by relatively fast nucleation followed by relatively slow growth (Tables 2 and 3). The forward rate constant for the isomerization step of growth, k_4, appears to be rate-limiting under most conditions. This observation suggests that presynaptic filaments assemble via multiple nucleation events, forming many short filaments rather than a few long ones. The need for many nucleation events, along with the strict requirement for UvsY in filament nucleation at high salt concentrations, helps to explain the fact that UvsY is needed in an approximately 1:1 stoichiometry with UvsX for optimal strand exchange activity.[7,14] It is also consistent with single-molecule studies of human RAD51 and *E. coli* RecA assembly on duplex DNA, which show that these recombinases rapidly form multiple nucleation sites.[25,30,31]

The displacement of Gp32 from ssDNA by UvsX and/or UvsY proteins is a relatively slow process, yet presynaptic filament assembly occurs rapidly enough to account for the observed rates of UvsX-catalyzed DNA strand exchange. At high UvsX concentrations in 50 mM NaCl and ATP, UvsX approaches half-saturation of the ssDNA within 1.5–2 min (Figure 4), which corresponds to the earliest times at which recombination intermediates appear in DNA strand exchange reactions performed under similar conditions.[7,28] The data suggest that partial saturation of ssDNA by UvsX protein is sufficient to initiate homologous pairing. At high UvsX concentrations in 200 mM NaCl with ATP and UvsY, UvsX approaches half-saturation of the ssDNA within 4–5 min (Figure 4). Early strand exchange and recombination-dependent replication products typically appear within 2–5 min under

dx.doi.org/10.1021/bi401060p | *Biochemistry* 2013, 52, 7878–7889

similar conditions and require concentrations of UvsX significantly lower than those required under UvsY-independent conditions.[7,13] The data suggest that relatively short, UvsY-stabilized filaments are preferred for the initiation of homologous pairing reactions, which are not limited by slow filament growth rates.

UvsX Recombinase Actively Displaces Gp32 from ssDNA. As illustrated in Figure 5, both nucleation and growth phases include isomerization steps (k_2 and k_4) in which Gp32 is ejected from the ssDNA. In our experiments with the Gp32F probe, values of k_2 and k_4 (Table 3) greatly exceed values of the rate constant for spontaneous dissociation of Gp32F from cooperative clusters (k_{-2} in Table 1) under all conditions examined. Therefore, UvsX does not passively occupy binding sites abandoned by Gp32; rather, it actively displaces Gp32 from the lattice. Without the challenge from UvsX, the preassembled Gp32F−ssDNA complex remains stable for >10 min without detectable dissociation (data not shown). Active displacement requires ATP (or ATPγS) binding by UvsX and also requires UvsY under high-salt conditions. One possible mechanism for active displacement is shown schematically in Figure 5. We propose that isomerization of UvsX not only displaces Gp32 from ssDNA locally but also remodels and destabilizes adjacent ends of Gp32 clusters, effectively increasing their off rate for dissociation from ssDNA.

Implications for Recombination in T4 and Other Systems. Presynaptic filament assembly involves an intricate choreography of protein−ssDNA and protein−protein interactions among recombinase, SSB, and mediator components of the homologous recombination machinery. Each interaction is modulated by solution variables, including ion concentrations and nucleotide ligands. These variables determine the efficiency of recombinase−SSB exchange on ssDNA and thereby dictate the requirement for mediator protein activities in filament assembly. In this study, we have quantified key aspects of the salt, nucleotide, and mediator protein effects that influence recombinase−SSB exchange during T4 presynaptic filament assembly. Results indicate that the efficiency of T4 presynaptic filament assembly *in vivo* is controlled by two major kinetic effects: (1) the requirement for UvsY mediator to stabilize the prenucleation complex formed by UvsX recombinase on Gp32-covered ssDNA and (2) the rate-limiting nature of filament growth. The data suggest that T4 *uvsY* mutant strains are recombination-deficient specifically because they cannot form UvsX prenucleation complexes under *in vivo* salt conditions. Our model predicts that it should be possible to isolate UvsX or Gp32 mutants, or to identify chemical agents, that suppress *uvsY* mutations by stabilizing the prenucleation complex. In this regard, a yeast Rad51-I345T mutant protein shows enhanced binding and stability to ss- and dsDNA, which can partially bypass the requirement for Rad55−Rad57 mediator proteins in DNA repair.[32] Conversely, agents that destabilize the prenucleation complex would be predicted to inhibit recombination *in vivo*.

Presynaptic filament structure and function are highly conserved among diverse species; likewise, SSB and mediator proteins are functionally conserved. Therefore, it seems probable that cellular recombination systems follow some of the same kinetic principles as those employed by the T4 system. Our kinetic studies suggest that UvsX and UvsY form many nucleation centers and short segments on the Gp32−ssDNA complex, and the dominance of filament nucleation argues for a kinetically competent discontinuous filament. A growing body of evidence suggests that discontinuous presynaptic filaments may be a general feature of all homologous recombination systems.[36] Single-molecule studies have demonstrated that RecA and Rad51 form multiple nucleation sites on either naked or SSB-covered DNA.[19,25,30,33] Rad51 forms protein patches with gaps on dsDNA molecules and typically forms irregular structures on ssDNA.[30,34] EM structures of human Rad51−Rad52 cofilaments reveal multiple individual Rad52 binding sites on Rad51-covered ssDNA.[35] Rad51 paralogs Rad55 and Rad57 in yeast and Rad51B and Rad51C in humans both appear to integrate into Rad51−ssDNA presynaptic filaments and protect them from disruption by antirecombination helicases Srs2 and Blm, respectively.[37,38] We propose that the formation of discontinuous filaments may be advantageous for their regulation by recombination mediator proteins, both at the level of nucleation (e.g., by classic mediators such as T4 UvsY, *E. coli* RecFOR, Rad52, or Brca2[4,36]) and at the level of segment stabilization (e.g., by Rad51 paralogs such as Rad55 and Rad57 or Rad51B and Rad51C). It seems possible that in humans the Rad51−ssDNA filament could be deliberately managed by Brca2 and Rad51B/Rad51C to form relatively short, stable segments that are optimized to promote recombination by a synthesis-dependent strand annealing (SDSA) mechanism that avoids genotoxic crossovers and genomic instability.[39] Bacteriophage T4 is proficient in SDSA, which is promoted *in vitro* by purified UvsX, UvsY, Gp32, and replication enzymes.[40] Mechanistic studies of this process are likely to inform studies of SDSA and related genome stability processes in humans and other organisms.

AUTHOR INFORMATION

Corresponding Author

*Department of Biochemistry, University of Vermont College of Medicine, 89 Beaumont Ave., Burlington, VT 05405. E-mail: smorrica@uvm.edu. Phone: (802) 656-8260.

Present Address

[§]J.L.: Department of Microbiology and Molecular Genetics, University of California, Davis, CA 95616.

Funding

Supported by National Institutes of Health Grants GM48847 to S.W.M. and HL63798 to C.L.B. J.L. was supported by a DOE-EPSCoR predoctoral fellowship in structural biology.

Notes

The authors declare no competing financial interest.

ABBREVIATIONS

ssDNA, single-stranded DNA; SSB, single-stranded DNA binding protein; RMP, recombination mediator protein; ATPγS, adenosine 5′-*O*-(3-thio)triphosphate.

ADDITIONAL NOTE

[a]Morrical, S. W., and Qian, N. Methods and Compositions for Optical Detection of Single-stranded Polynucleotides. U.S. Patent 7,544,469. Morrical, S. W., and Qian, N. Methods and Compositions for Optical Detection of Single-stranded Polynucleotides. International Patent Application PCT/US2004/000665.

REFERENCES

(1) Bianco, P. R., Tracy, R. B., and Kowalczykowski, S. C. (1998) DNA strand exchange proteins: A biochemical and physical comparison. *Front. Biosci. 3*, 570−603.

(2) Khanna, K. K., and Jackson, S. P. (2001) DNA double-strand breaks: Signaling, repair and the cancer connection. *Nat. Genet. 27*, 247−254.

(3) Jasin, M. (2002) Homologous repair of DNA damage and tumorigenesis: The BRCA connection. *Oncogene 21*, 8981−8993.

(4) Beernink, H. T., and Morrical, S. W. (1999) RMPs: Recombination/replication mediator proteins. *Trends Biochem. Sci. 24*, 385−389.

(5) Bleuit, J. S., Xu, H., Ma, Y., Wang, T., Liu, J., and Morrical, S. W. (2001) Mediator proteins orchestrate enzyme-ssDNA assembly during T4 recombination-dependent DNA replication and repair. *Proc. Natl. Acad. Sci. U.S.A. 98*, 8298−8305.

(6) Liu, J., Qian, N., and Morrical, S. W. (2006) Dynamics of bacteriophage T4 presynaptic filament assembly from extrinsic fluorescence measurements of Gp32-single-stranded DNA interactions. *J. Biol. Chem. 281*, 26308−26319.

(7) Bleuit, J. S., Ma, Y., Munro, J., and Morrical, S. W. (2004) Mutations in a conserved motif inhibit single-stranded DNA binding and recombination mediator activities of bacteriophage T4 UvsY protein. *J. Biol. Chem. 279*, 6077−6086.

(8) Liu, J., Bond, J. P., and Morrical, S. W. (2006) Mechanism of presynaptic filament stabilization by the bacteriophage T4 UvsY recombination mediator protein. *Biochemistry 45*, 5493−5502.

(9) Sweezy, M. A., and Morrical, S. W. (1999) Biochemical interactions within a ternary complex of the bacteriophage T4 recombination proteins uvsY and gp32 bound to single-stranded DNA. *Biochemistry 38*, 936−944.

(10) Kodadek, T., Gan, D. C., and Stemke-Hale, K. (1989) The phage T4 uvsY recombination protein stabilizes presynaptic filaments. *J. Biol. Chem. 264*, 16451−16457.

(11) Harris, L. D., and Griffith, J. D. (1989) UvsY protein of bacteriophage T4 is an accessory protein for in vitro catalysis of strand exchange. *J. Mol. Biol. 206*, 19−27.

(12) Yonesaki, T., and Minagawa, T. (1989) Synergistic action of three recombination gene products of bacteriophage T4, uvsX, uvsY, and gene 32 proteins. *J. Biol. Chem. 264*, 7814−7820.

(13) Morrical, S. W., and Alberts, B. M. (1990) The UvsY protein of bacteriophage T4 modulates recombination-dependent DNA synthesis in vitro. *J. Biol. Chem. 265*, 15096−15103.

(14) Yassa, D. S., Chou, K. M., and Morrical, S. W. (1997) Characterization of an amino-terminal fragment of the bacteriophage T4 uvsY recombination protein. *Biochimie 79*, 275−285.

(15) Formosa, T., and Alberts, B. M. (1986) Purification and characterization of the T4 bacteriophage uvsX protein. *J. Biol. Chem. 261*, 6107−6118.

(16) Cunningham, R. P., and Berger, H. (1977) Mutations affecting genetic recombination in bacteriophage T4D. I. Pathway analysis. *Virology 80*, 67−82.

(17) Melamede, R. J., and Wallace, S. S. (1977) Properties of the nonlethal recombinational repair x and y mutants of bacteriophage T4. II. DNA synthesis. *J. Virol. 24*, 28−40.

(18) Lohman, T. M., and Kowalczykowski, S. C. (1981) Kinetics and mechanism of the association of the bacteriophage T4 gene 32 (helix destabilizing) protein with single-stranded nucleic acids. Evidence for protein translocation. *J. Mol. Biol. 152*, 67−109.

(19) Bell, J. C., Plank, J. L., Dombrowski, C. C., and Kowalczykowski, S. C. (2012) Direct imaging of RecA nucleation and growth on single molecules of SSB-coated ssDNA. *Nature 491*, 274−278.

(20) Kuzmic, P. (1996) Program DYNAFIT for the analysis of enzyme kinetic data: Application to HIV proteinase. *Anal. Biochem. 237*, 260−273.

(21) Ando, R. A., and Morrical, S. W. (1998) Single-stranded DNA binding properties of the UvsX recombinase of bacteriophage T4: Binding parameters and effects of nucleotides. *J. Mol. Biol. 283*, 785−796.

(22) Farb, J. N., and Morrical, S. W. (2009) Role of allosteric switch residue histidine 195 in maintaining active-site asymmetry in presynaptic filaments of bacteriophage T4 UvsX recombinase. *J. Mol. Biol. 385*, 393−404.

(23) Maher, R. L., and Morrical, S. W. (2013) Coordinated binding of single-stranded and double-stranded DNA by UvsX recombinase. *PLoS One 8*, e66654.

(24) Sweezy, M. A., and Morrical, S. W. (1997) Single-stranded DNA binding properties of the uvsY recombination protein of bacteriophage T4. *J. Mol. Biol. 266*, 927−938.

(25) Galletto, R., Amitani, I., Baskin, R. J., and Kowalczykowski, S. C. (2006) Direct observation of individual RecA filaments assembling on single DNA molecules. *Nature 443*, 875−878.

(26) Branagan, A. M., Maher, R. L., and Morrical, S. W. (2012) Assembly and dynamics of Gp59-Gp32-single-stranded DNA (ssDNA), a DNA helicase loading complex required for recombination-dependent replication in bacteriophage T4. *J. Biol. Chem. 287*, 19070−19081.

(27) Pant, K., Karpel, R. L., Rouzina, I., and Williams, M. C. (2005) Salt dependent binding of T4 gene 32 protein to single and double-stranded DNA: Single molecule force spectroscopy measurements. *J. Mol. Biol. 349*, 317−330.

(28) Kodadek, T., Wong, M. L., and Alberts, B. M. (1988) The mechanism of homologous DNA strand exchange catalyzed by the bacteriophage T4 uvsX and gene 32 proteins. *J. Biol. Chem. 263*, 9427−9436.

(29) Menetski, J. P., and Kowalczykowski, S. C. (1985) Interaction of recA protein with single-stranded DNA. Quantitative aspects of binding affinity modulation by nucleotide cofactors. *J. Mol. Biol. 181*, 281−295.

(30) Modesti, M., Ristic, D., van der Heijden, T., Dekker, C., van Mameren, J., Peterman, E. J., Wuite, G. J., Kanaar, R., and Wyman, C. (2007) Fluorescent human RAD51 reveals multiple nucleation sites and filament segments tightly associated along a single DNA molecule. *Structure 15*, 599−609.

(31) van der Heijden, T., Seidel, R., Modesti, M., Kanaar, R., Wyman, C., and Dekker, C. (2007) Real-time assembly and disassembly of human RAD51 filaments on individual DNA molecules. *Nucleic Acids Res. 35*, 5646−5657.

(32) Fortin, G. S., and Symington, L. S. (2002) Mutations in yeast Rad51 that partially bypass the requirement for Rad55 and Rad57 in DNA repair by increasing the stability of Rad51-DNA complexes. *EMBO J. 21*, 3160−3170.

(33) Hilario, J., Amitani, I., Baskin, R. J., and Kowalczykowski, S. C. (2009) Direct imaging of human Rad51 nucleoprotein dynamics on individual DNA molecules. *Proc. Natl. Acad. Sci. U.S.A. 106*, 361−368.

(34) Ristic, D., Modesti, M., van der Heijden, T., van Noort, J., Dekker, C., Kanaar, R., and Wyman, C. (2005) Human Rad51 filaments on double- and single-stranded DNA: Correlating regular and irregular forms with recombination function. *Nucleic Acids Res. 33*, 3292−3302.

(35) Van Dyck, E., Hajibagheri, N. M., Stasiak, A., and West, S. C. (1998) Visualisation of human rad52 protein and its complexes with hRad51 and DNA. *J. Mol. Biol. 284*, 1027−1038.

(36) Liu, J., Ehmsen, K. T., Heyer, W. D., and Morrical, S. W. (2011) Presynaptic filament dynamics in homologous recombination and DNA repair. *Crit. Rev. Biochem. Mol. Biol. 46*, 240−270.

(37) Liu, J., Renault, L., Veaute, X., Fabre, F., Stahlberg, H., and Heyer, W. D. (2011) Rad51 paralogues Rad55-Rad57 balance the antirecombinase Srs2 in Rad51 filament formation. *Nature 479*, 245−248.

(38) Amunugama, R., Groden, J., and Fishel, R. (2013) The HsRAD51B-HsRAD51C stabilizes the HsRAD51 nucleoprotein filament. *DNA Repair 12*, 723−732.

(39) Maher, R. L., Branagan, A. M., and Morrical, S. W. (2011) Coordination of DNA replication and recombination activities in the maintenance of genome stability. *J. Cell. Biochem. 112*, 2672−2682.

(40) Liu, J., and Morrical, S. W. (2010) Assembly and dynamics of the bacteriophage T4 homologous recombination machinery. *Virol. J.* 7, 357.